antioxidants

MDPI

Article

Salvianolic Acid B Alleviates Lipopolysaccharide-Induced Intestinal Barrier Dysfunction by Restoring Epithelial Proliferation–Apoptosis Balance and Modulating the Gut Microbiota

Yuxin Jiang [1,†], Huan Xie [2,3,†], Hao Zhang [4], Jinsong Zhang [1], Yanfei Yu [2,3], Yanan Chen [1,*], Hao Wang [2,*], Chenhuan Lai [1] and Qiang Yong [1]

[1] National Key Laboratory for the Development and Utilization of Forest Food Resources, Nanjing Forestry University, Nanjing 210037, China
[2] Key Laboratory of Veterinary Biological Engineering and Technology, Ministry of Agriculture and Rural Affairs, Institute of Veterinary Medicine, Jiangsu Academy of Agricultural Sciences, Nanjing 210014, China
[3] College of Veterinary Medicine, Nanjing Agricultural University, Nanjing 210095, China
[4] College of Animal Science & Technology, Nanjing Agricultural University, Nanjing 210095, China
* Correspondence: chenyn18@njfu.edu.cn (Y.C.); wanghao0713@jaas.ac.cn (H.W.)
† These authors contributed equally to this work.

Abstract

Background: Intestinal epithelial barrier dysfunction, a major consequence of inflammatory and oxidative stress, contributes to enteric disorder progression. Salvianolic acid B (SAB), a prominent water-soluble phenolic compound in *Salvia miltiorrhiza*, shows intestinal protective potential, but the underlying mechanisms remain unclear. Methods: This study investigated the protective effects of SAB on intestinal barrier function using a lipopolysaccharide (LPS)-challenged piglet model and LPS-stimulated IPEC-J2 cells. Results: SAB alleviated LPS-induced intestinal injury, evidenced by reduced plasma diamine oxidase and D-lactate levels, improved intestinal morphology, decreased pro-inflammatory cytokines, and enhanced antioxidant capacity. SAB also strengthened intestinal barrier integrity by increasing goblet cell number and mucin 2 levels and upregulating tight junction protein expression. Moreover, SAB restored epithelial proliferation–apoptosis balance and increased PI3K/AKT/mTOR phosphorylation. Molecular docking and molecular dynamics simulations predicted a stable SAB–PI3Kα/p110α interaction, whereas LY294002 treatment attenuated SAB-mediated restoration of epithelial renewal and barrier integrity in LPS-treated IPEC-J2 cells. SAB also altered the jejunal microbial composition, including higher relative abundance of *Streptococcus* and lower relative abundance of *Escherichia-Shigella*, together with increased jejunal acetate and lactate concentrations. Conclusions: SAB alleviates inflammation-associated intestinal barrier dysfunction by restoring epithelial proliferation–apoptosis balance and regulating the microbiota–metabolite profile.

Keywords: Salvianolic acid B; intestinal barrier dysfunction; epithelial proliferation and apoptosis; gut microbiota

Check for updates

Academic Editor: Jicheng Zhan

Received: 2 September 2026
Revised: 30 October 2026
Accepted: 31 October 2026
Published: 3 November 2026

Copyright: © 2026 by the authors. Licensee MDPI, Basel, Switzerland. This article is an open access article distributed under the terms and conditions of the Creative Commons Attribution (CC BY) license.

1. Introduction

Intestinal epithelial barrier dysfunction is a hallmark pathological feature of numerous enteric disorders, including inflammatory bowel disease, infection-associated enteritis, and inflammation-related mucosal injury [1]. Loss of epithelial integrity increases mucosal exposure

to luminal antigens, microbial products, and potentially harmful metabolites, thereby intensifying local inflammation and tissue damage [2]. Oxidative stress commonly accompanies intestinal inflammation and can further compromise epithelial barrier integrity by overwhelming endogenous antioxidant defenses and promoting lipid peroxidation [3,4]. Therefore, identifying plant-derived bioactive compounds that help maintain epithelial homeostasis may represent a useful strategy for protecting intestinal barrier function during inflammatory stress.

The intestinal epithelium forms the primary physical and functional boundary between the host and the gut lumen, and its integrity depends not only on intact intercellular junctions but also on continuous epithelial renewal along the crypt–villus axis [5]. Under physiological conditions, epithelial proliferation and apoptosis are tightly coordinated, whereas inflammatory stress can disrupt this balance, leading to impaired epithelial renewal, villus atrophy, and barrier dysfunction [6]. Among the signaling networks involved in epithelial homeostasis, the phosphatidylinositol 3-kinase (PI3K)/protein kinase B (AKT)/mammalian target of rapamycin (mTOR) pathway is a central regulator of cell growth, survival, metabolism, and tissue repair [7,8]. Dysregulated PI3K/AKT/mTOR signaling has been linked to defective epithelial renewal and delayed mucosal repair in several models of intestinal injury [9,10]. Meanwhile, the gut microbiota contributes to intestinal homeostasis through colonization resistance, mucosal immune regulation, and the generation of microbial metabolites, such as short-chain fatty acids (SCFAs) [11,12]. Intestinal inflammation is frequently accompanied by microbial dysbiosis and altered metabolite production, which may further compromise epithelial and mucosal homeostasis [13,14]. Thus, coordinated maintenance of epithelial renewal and gut microbial homeostasis may be important for preserving intestinal barrier function and facilitating mucosal recovery.

Salvianolic acid B (SAB) is a predominant water-soluble phenolic compound in *Salvia miltiorrhiza* with antioxidant, anti-inflammatory, and cytoprotective properties [15,16]. Previous studies have shown that SAB mitigates inflammatory injury through multiple signaling mechanisms, including suppression of the TLR4/MyD88/MAPK cascade [17], modulation of NF-κB RelA activity [18], and inhibition of NF-κB/NLRP3 signaling [19]. SAB has also been reported to ameliorate experimental colitis and intestinal ischemia–reperfusion injury [17,20], suggesting its potential to preserve epithelial integrity during inflammatory stress. However, the mechanisms underlying the intestinal protective effects of SAB have not been fully elucidated. In particular, whether SAB restores epithelial proliferation–apoptosis balance and modulates the gut microbiota and associated metabolites during inflammation-associated intestinal barrier injury remains unclear.

Lipopolysaccharide (LPS), an outer membrane component of Gram-negative bacteria, is well documented to induce systemic and intestinal inflammatory injury in several experimental models [21]. Pigs are highly relevant models for intestinal research because they share substantial similarities with humans in gastrointestinal anatomy, digestive physiology, and gut microbial characteristics [22]. LPS-challenged piglets therefore provide a useful model for evaluating intestinal responses to bioactive compounds [23,24]. In the current research, we combined an LPS-challenged piglet model with an LPS-stimulated porcine intestinal epithelial cell line (IPEC-J2) to explore the protective effects and underlying mechanisms of SAB. We hypothesized that SAB attenuates inflammation-associated intestinal barrier injury by restoring proliferation–apoptosis balance through PI3K/AKT/mTOR signaling, accompanied by modulation of the gut microbiota–metabolite profile. The present study aimed to elucidate the mechanisms underlying SAB-mediated intestinal protection and provide mechanistic insights into its potential application as a plant-derived bioactive compound.

2. Materials and Methods

2.1. Animal Experiment

The animal study protocol was approved by the Institutional Animal Care and Use Committee of Nanjing Forestry University (approval no. 2024020).

Eighteen weaned male Duroc × Landrace × Large White piglets (initial body weight, 10.26 ± 0.24 kg) were allocated randomly to three treatments (n = 6): non-challenged control (CON-SS), LPS-challenged control (CON-LPS), and LPS-challenged pigs receiving SAB (SAB-LPS). The sample size of six piglets per group was selected based on previous published studies using similar experimental designs [25,26]. No formal a priori power calculation was performed. Animals were maintained individually from 35 to 56 days of age and had ad libitum access to feed and water. Piglets in the CON-SS and CON-LPS groups received the basal diet, whereas piglets in the SAB-LPS group received the basal diet containing 200 mg SAB/kg diet (purity ≥98%; CAS no. 121521-90-2; Tokyo Chemical Industry Co., Ltd., Shanghai, China). At 56 days of age, piglets in the CON-LPS and SAB-LPS groups were intraperitoneally injected with LPS (25 μg/kg body weight; CAS No. 93572-42-0; Sigma-Aldrich, St. Louis, MO, USA), whereas CON-SS piglets received an equivalent volume of sterile saline. At 6 h after LPS challenge, blood, jejunal tissue, jejunal digesta, and mucosal samples were collected. Plasma was prepared for diamine oxidase (DAO) and D-lactate analyses. Mid-jejunal segments were collected for histological and immunofluorescence analyses, jejunal digesta for microbiota and metabolite measurements, and mucosal scrapings for molecular analyses. Detailed procedures for sample collection and processing are provided in Supplementary Methods S1. The LPS dose and sampling time were selected based on established porcine LPS-challenge models, in which intraperitoneal LPS administration induced marked intestinal injury and inflammatory responses within 4–6 h after challenge [25,27]. The dietary SAB dose (200 mg/kg) was selected based on our previous studies in LPS-challenged piglets, in which supplementation with 200 mg/kg SAB effectively attenuated inflammatory injury in the liver and spleen [18,28]. The basal diet was formulated following NRC (2012) recommendations (Table S1).

2.2. Determination of DAO and D-Lactate Levels

Plasma DAO activity (Nanjing Jiancheng Bioengineering Institute; Nanjing, Jiangsu, China) and D-lactate levels (Sigma-Aldrich) were quantified with corresponding colorimetric kits, respectively.

2.3. Determination of Cytokines, Mucin 2, and Antioxidant Parameters

Jejunal mucosal samples were homogenized in ice-cold physiological saline and centrifuged at 3500× g for 15 min at 4 °C. The resulting supernatants were collected for subsequent analyses. The concentrations of tumor necrosis factor-alpha (TNF-α), interleukin-1 beta (IL-1β), interleukin-6 (IL-6), and mucin 2 were determined using porcine-specific ELISA kits (Cusabio, Wuhan, China). Superoxide dismutase (SOD) and glutathione peroxidase (GPX) activities and malondialdehyde (MDA) content were measured using commercial assay kits (Nanjing Jiancheng Bioengineering Institute).

2.4. Histological and Immunofluorescence Staining

Paraformaldehyde-fixed jejunal tissues were paraffin-embedded and cut into 5-μm sections. For conventional histology, sections were subjected to hematoxylin and eosin (H&E) staining. Histopathological injury was scored according to villus integrity, epithelial shedding, mucosal edema, and inflammatory cell infiltration. Goblet cells were visualized by Alcian blue–periodic acid-Schiff (AB-PAS) staining. After removal of paraffin and rehydration, sections were exposed to Alcian blue, followed by oxidation with 0.5%

periodic acid and incubation with Schiff's reagent in darkness. Mayer's hematoxylin was used for counterstaining before dehydration, clearing, and mounting. Villus height (VH), crypt depth (CD), VH/CD ratio, and AB-PAS-positive goblet cells were determined from 10 randomly selected, well-oriented villus–crypt units per animal.

For immunofluorescence, paraffin sections underwent citrate-based heat-mediated antigen retrieval and were incubated with 5% goat serum. Primary antibodies against Ki67, occludin, or zonula occludens-1 (ZO-1) were applied overnight at 4 °C. Sections were subsequently incubated with the corresponding Alexa Fluor-labeled secondary antibodies for 1 h in darkness, followed by 4′,6-diamidino-2-phenylindole (DAPI) nuclear counterstaining. Ki67-positive cells were counted in 10 well-oriented villus–crypt units from each sample, whereas occludin and ZO-1 fluorescence intensities were quantified from five randomly chosen fields. Antibody details are listed in Table S2.

Apoptotic cells in jejunal sections were visualized using a terminal deoxynucleotidyl transferase dUTP nick-end labeling (TUNEL) kit (Vazyme, Nanjing, China). Sections received proteinase K treatment for 20 min and were subsequently subjected to the labeling reaction for 1 h at 37 °C before DAPI counterstaining. TUNEL-positive cells were enumerated in 10 well-oriented villus–crypt units per sample. Microscopic images were obtained using Olympus fluorescence microscopy (BX43; Evident Corporation, Tokyo, Japan), and quantitative analysis was conducted with Image-Pro Plus (version 6.0.0.260).

2.5. Cell Culture and Treatment

IPEC-J2 cells (Procell Life Science & Technology; Wuhan, Hubei, China) were cultured in DMEM/F12 medium supplemented with 10% fetal bovine serum and 1% penicillin–streptomycin (Gibco; Grand Island, NY, USA) at 37 °C in a humidified incubator with 5% CO_2. Cells at passages 5–15 were used for experiments.

To determine the working concentration of SAB, cell viability was first assessed after treatment with increasing dosages of SAB (0–500 μM) for 24 h using the CCK-8 assay. To identify an effective concentration under inflammatory conditions, cells were pretreated with SAB (0–200 μM) for 2 h, followed by co-treatment with SAB at the corresponding concentrations and LPS (1 μg/mL) for an additional 24 h. Cell viability was then assessed using the CCK-8 assay. Based on these results, 25 μM SAB was selected for subsequent mechanistic studies (Figure S1).

For PI3K inhibition experiments, cells were pre-incubated with the PI3K inhibitor LY294002 (5 μM; MedChemExpress; Shanghai, China) for 1 h, followed by SAB (25 μM) treatment for 2 h. The medium was then replaced with fresh medium containing SAB (25 μM) and LPS (1 μg/mL) for an additional 24 h of co-treatment. The concentration and pretreatment duration of LY294002 were selected based on previous studies [29,30] and preliminary experiments showing that this condition reduced AKT and mTOR phosphorylation without significantly affecting IPEC-J2 cell viability (Figure S2). The experimental groups included Control, SAB, LPS, LPS + SAB, and LPS + SAB + LY294002. The SAB group followed the same treatment schedule as the LPS + SAB group, except that LPS was omitted from the fresh SAB-containing medium. The final vehicle concentration was kept consistent across all experimental groups.

2.6. Assessment of Epithelial Barrier Function

IPEC-J2 cells were cultured on 0.4-μm Transwell inserts until a confluent monolayer was established, as indicated by a transepithelial electrical resistance (TEER) of approximately 500 $\Omega \cdot cm^2$. Following the indicated treatments, epithelial barrier function was evaluated by TEER measurement and apical-to-basolateral transport of 4-kDa fluorescein isothiocyanate-dextran (FD4; 1 mg/mL, 2 h; Sigma-Aldrich). Detailed procedures are

provided in Supplementary Methods S2. TEER values were expressed in $\Omega \cdot cm^2$, whereas FD4 permeability was expressed as fold changes relative to the control group.

2.7. 5-Ethynyl-2′-Deoxyuridine (EdU) Proliferation Assay

Cell proliferation was quantified with an AF594 EdU assay (Beyotime; Haimen, China). After treatment with LPS, SAB, and/or LY294002, cells were fixed in 4% paraformaldehyde and permeabilized with 0.3% Triton X-100. Incorporated EdU was fluorescently labeled using the Azide 594 click-reaction mixture for 30 min in darkness. Hoechst 33342 was used to visualize nuclei. The percentage of EdU-positive nuclei was calculated from microscopic images.

2.8. Apoptosis Analysis by Flow Cytometry

Apoptosis was quantified by Annexin V–fluorescein isothiocyanate/propidium iodide (Annexin V-FITC/PI; Beyotime) staining followed by flow cytometry. Following the indicated treatments, IPEC-J2 cells were harvested, washed, and resuspended, followed by staining with Annexin V-FITC and PI for 15 min at room temperature in the dark. Fluorescence was acquired on a BD flow cytometer (Franklin Lakes, NJ, USA). The apoptosis rate was expressed as the percentage of apoptotic cells among the total analyzed cells.

2.9. Molecular Docking and Molecular Dynamics (MD) Simulations

The structure of SAB (PubChem CID: 5281793) and the human PI3Kα catalytic subunit p110α (*PIK3CA*; PDB 9CMV, chain A) were used for molecular docking with AutoDock Vina 1.2.3. The pose with the lowest Vina docking score was subjected to a single 100-ns molecular dynamics (MD) simulation using AMBER 24. Structural dynamics and binding energetics were analyzed, with the latter estimated using molecular mechanics/generalized Born surface area (MM/GBSA) calculations without an entropy contribution. Detailed procedures are provided in Supplementary Methods S3.

2.10. Total RNA Extraction and Quantitative Real-Time PCR (RT-qPCR) Analysis

RNA was isolated from jejunal tissue and IPEC-J2 cells with TRIzol and reverse-transcribed using PrimeScript RT Master Mix (TaKaRa; Kyoto, Japan). RT-qPCR amplification was carried out on a QuantStudio 5 Real-Time PCR System (Applied Biosystems; Foster City, CA, USA) employing TB Green Premix Ex Taq (TaKaRa). The $2^{-\Delta\Delta Ct}$ method was employed to calculate relative mRNA levels, with *ACTB* serving as the internal reference. Primer sequences are listed in Table S3. Relative mRNA expression was expressed as fold changes relative to the control group.

2.11. Western Blot Analysis

Proteins were extracted from jejunal tissue and IPEC-J2 cells in RIPA buffer containing protease/phosphatase inhibitor cocktails (Beyotime) and quantified by BCA assay (Beyotime). Equal protein lysates were resolved on 8–12% SDS-PAGE gels and wet-transferred to PVDF membranes. Following blocking (5% BSA, 1 h), membranes were probed with primary antibodies (4 °C, overnight) and HRP-secondary antibodies (room temperature, 1 h). Chemiluminescent signals were captured using a Bio-Rad ChemiDoc system (Hercules, CA, USA) and quantified with Gel-Pro Analyzer. Phosphorylated PI3K, AKT, and mTOR were normalized to their corresponding total protein levels, whereas occludin and ZO-1 were normalized to β-tubulin. Antibodies are listed in Table S2. The normalized protein levels were expressed as fold changes relative to the control group.

2.12. Microbial DNA Extraction and 16S rRNA Gene Sequencing

Jejunal digesta from each piglet were processed and analyzed independently, with six biological replicates per treatment group. Microbial DNA was extracted from jejunal digesta

using a commercial kit (Tiangen Biotech, Beijing, China). The V3–V4 region of the bacterial 16S rRNA gene was amplified using primers 338F (5′-ACTCCTACGGGAGGCAGCAG-3′) and 806R (5′-GGACTACHVGGGTWTCTAAT-3′), and the purified amplicons were sequenced on an Illumina NextSeq 2000 platform (Illumina, Inc., San Diego, CA, USA). Raw paired-end reads were quality-filtered using fastp and merged using FLASH (version 1.2.11). Operational taxonomic units (OTUs) were clustered at 97% sequence identity using UPARSE (version 7.0.1090), and representative sequences were taxonomically classified against the SILVA 138 database using the RDP Classifier (version 2.11) with a 70% confidence threshold. To normalize sequencing depth across samples, the OTU table was rarefied to 20,000 sequences per sample before downstream analyses. Analyses were performed using the Majorbio Cloud Platform (Shanghai, China). Alpha diversity was assessed using the Sobs, Chao, Ace, Shannon, and Simpson indices. Pairwise differences in alpha-diversity indices among the three groups were assessed using the Wilcoxon rank-sum test, with false discovery rate (FDR) correction for multiple comparisons. Beta diversity was evaluated by principal coordinate analysis (PCoA) based on Bray–Curtis dissimilarities, and differences in community structure were assessed using Adonis analysis. Pairwise differences in taxon relative abundances at the phylum and genus levels were assessed using the Wilcoxon rank-sum test with FDR correction for multiple testing. Differential taxa were further explored using linear discriminant analysis effect size (LEfSe), with a linear discriminant analysis (LDA) score > 2.0 and $p < 0.05$ as thresholds. The raw sequencing data are available in the NCBI Sequence Read Archive under BioProject accession number PRJNA1519105.

2.13. Determination of Jejunal SCFAs and Lactate

Jejunal digesta were analyzed for acetate, propionate, and butyrate using gas chromatography with crotonic acid as an internal standard. Total SCFA concentration was calculated as the sum of acetate, propionate, and butyrate. Lactate was quantified separately by high-performance liquid chromatography using an external calibration curve. Detailed information is provided in Supplementary Methods S4.

2.14. Statistical Analysis

For animal experiments, *n* represents the number of individual animals, whereas for in vitro experiments, *n* represents independent biological replicates unless otherwise specified. Statistical analyses were performed using GraphPad Prism 10.0. Except for microbial community data, differences among groups were analyzed using one-way analysis of variance followed by Tukey's multiple-comparison test. Spearman's rank correlation analysis was carried out to evaluate associations among bacterial genera, microbial metabolites, and host barrier-related parameters. Data are presented as mean ± standard error of the mean (SEM), unless otherwise indicated. $p < 0.05$ was considered statistically significant.

3. Results

3.1. SAB Alleviates Intestinal Barrier Injury in LPS-Challenged Piglets

As shown in Figure 1A,B, plasma DAO activity and D-lactate concentration were significantly higher in the CON-LPS group than in the CON-SS group ($p < 0.05$). Histological analysis revealed marked morphological disruption in the jejunum of LPS-challenged piglets, characterized by villus atrophy, epithelial cell shedding, and mucosal edema (Figure 1C). Consistently, the histopathological injury score was markedly increased, whereas VH and the VH/CD ratio were reduced following LPS challenge ($p < 0.05$; Figure 1E–H). Meanwhile, LPS reduced goblet cell abundance, jejunal mucin 2 levels, and the fluorescence intensities of occludin and ZO-1 ($p < 0.05$; Figure 1C,D,I–L). These observations suggested that LPS incurred apparent intestinal barrier injury. In contrast,

SAB supplementation decreased plasma DAO activity and D-lactate concentration compared with the CON-LPS group ($p < 0.05$). SAB also substantially preserved jejunal mucosal structure, accompanied by a reduced histopathological injury score and restored VH ($p < 0.05$). Moreover, SAB replenished goblet cell numbers and mucin 2 levels and increased occludin and ZO-1 fluorescence intensities ($p < 0.05$). Collectively, these data demonstrate that SAB alleviates LPS-induced intestinal barrier injury and preserves mucosal integrity.

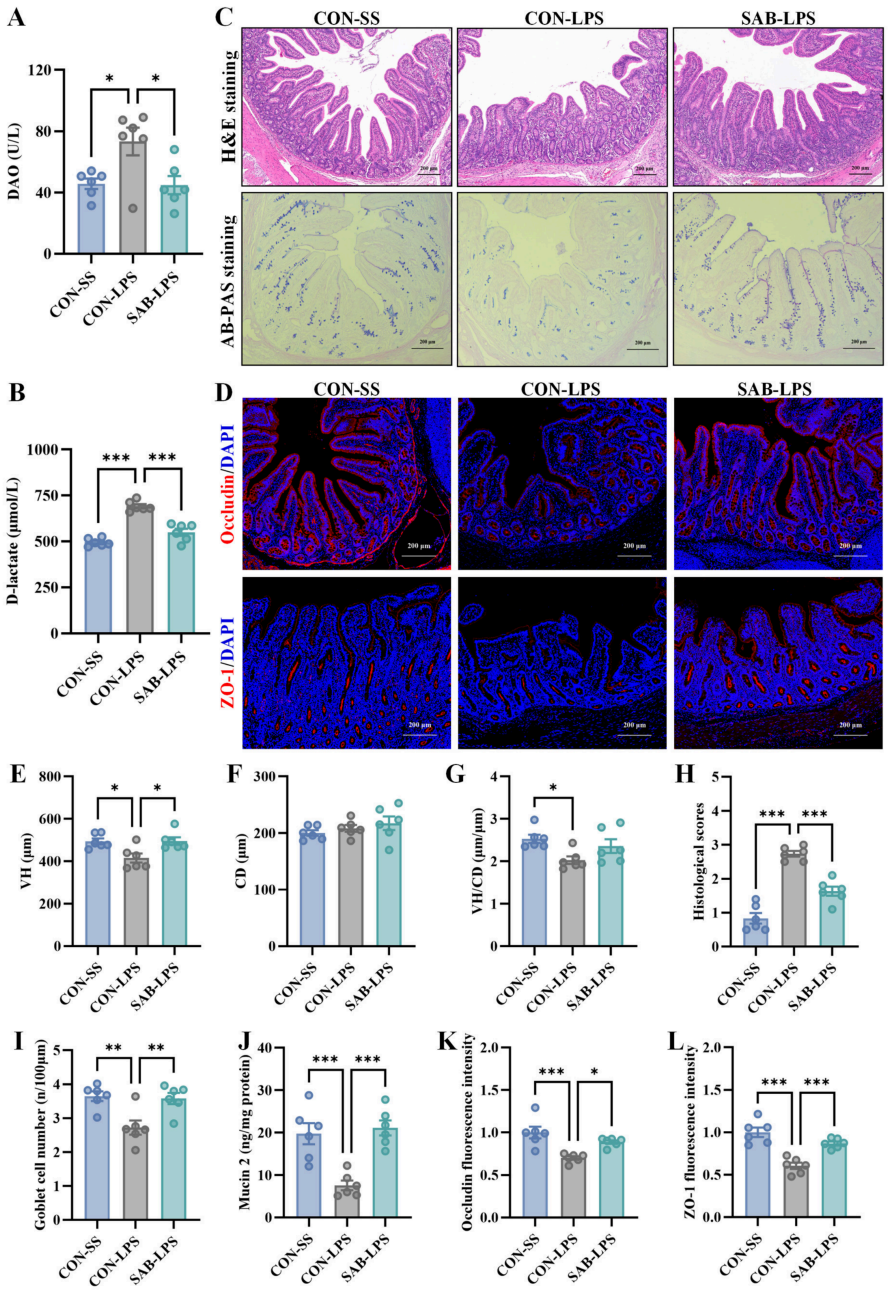


Figure 1. SAB alleviates intestinal barrier injury in LPS-challenged piglets. (**A**,**B**) Plasma DAO activity and D-lactate concentration; (**C**) Representative H&E- and AB-PAS-stained jejunal sections (scale bar = 200 μm); (**D**) Representative immunofluorescence images of occludin and ZO-1 in the jejunum (scale bar = 200 μm); (**E**–**H**) Jejunal VH, CD, VH/CD ratio, and histopathological injury score; (**I**) Goblet cell number; (**J**) Jejunal mucin 2 level; (**K**,**L**) Relative fluorescence intensities of occludin and ZO-1. Data are presented as mean ± SEM ($n = 6$). * $p < 0.05$, ** $p < 0.01$, *** $p < 0.001$.

3.2. SAB Attenuates Jejunal Inflammation and Improves Antioxidant Status in LPS-Challenged Piglets

Given that excessive inflammatory responses and impaired antioxidant defenses are closely associated with intestinal barrier disruption, we next evaluated jejunal pro-inflammatory cytokines and antioxidant parameters. LPS challenge markedly elevated TNF-α, IL-1β, and IL-6 concentrations in the jejunum ($p < 0.05$; Figure 2A–C). Meanwhile, LPS reduced SOD and GPX activities and increased MDA content ($p < 0.05$; Figure 2D–F). However, SAB supplementation significantly suppressed TNF-α and IL-1β overproduction, restored SOD and GPX activities, and reduced MDA content compared with the CON-LPS group ($p < 0.05$). These data indicate that SAB attenuates LPS-induced jejunal inflammation, enhances antioxidant defenses, and reduces lipid peroxidation.

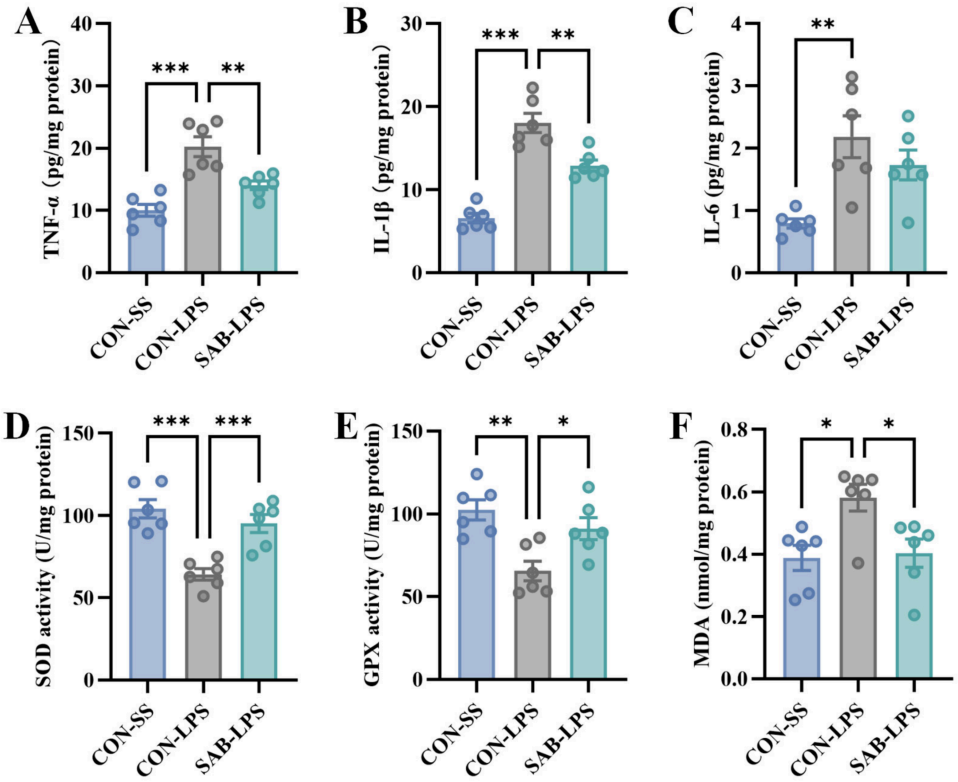


Figure 2. SAB attenuates jejunal inflammation and improves antioxidant status in LPS-challenged piglets. (**A**–**C**) Jejunal mucosal concentrations of TNF-α, IL-1β, and IL-6; (**D**,**E**) Jejunal SOD and GPX activities; (**F**) Jejunal MDA content. Data are presented as mean ± SEM ($n = 6$). * $p < 0.05$, ** $p < 0.01$, *** $p < 0.001$.

3.3. SAB Restores the Epithelial Proliferation–Apoptosis Balance in the Jejunum of LPS-Challenged Piglets

Given that the equilibrium between proliferation and apoptosis of intestinal epithelial cells is crucial for preserving barrier function, we assessed the effects of SAB on epithelial proliferation and apoptosis. LPS challenge significantly inhibited epithelial proliferation and triggered widespread apoptosis, as indicated by a robust decline in Ki67-positive cells and a substantial increase in TUNEL-positive cells throughout the jejunal mucosa ($p < 0.05$; Figure 3A–D). Consistently, RT-qPCR analysis suggested that LPS reduced the mRNA expression of the proliferation-associated markers, proliferating cell nuclear antigen (*PCNA*) and cyclin D1 (*CCND1*), and the anti-apoptotic gene B-cell lymphoma 2 (*BCL2*), while increasing the mRNA expression of the pro-apoptotic gene BCL2-associated X protein (*BAX*) ($p < 0.05$; Figure 3E). However, SAB partially reversed these LPS-induced alterations, as shown by increased Ki67-positive cells, decreased TUNEL-positive cells, and restored *PCNA*, *BCL2*,

and *BAX* expression ($p < 0.05$). Together, these results indicate that SAB improves epithelial proliferation–apoptosis balance during acute LPS-induced intestinal injury.

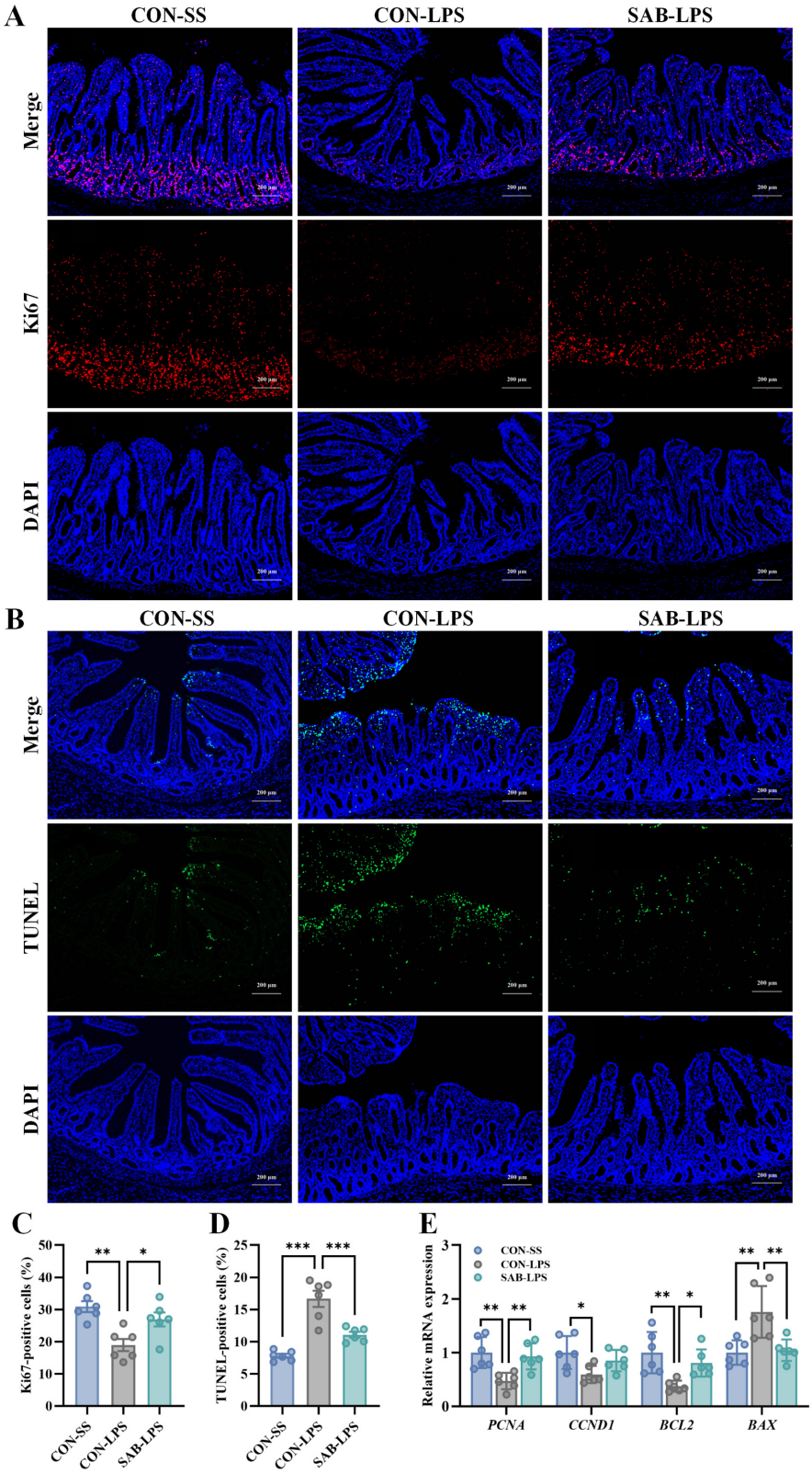


Figure 3. SAB promotes epithelial cell proliferation and inhibits apoptosis in the jejunum of LPS-challenged piglets. (**A**) Representative immunofluorescence images of Ki67 staining in jejunal sections (scale bar

= 200 μm); (**B**) Representative TUNEL staining images of jejunal sections (scale bar = 200 μm); (**C**) Quantification of Ki67-positive cells; (**D**) Quantification of TUNEL-positive cells; (**E**) Relative mRNA expression of proliferation- and apoptosis-associated genes. Data are presented as mean ± SEM (n = 6). * $p < 0.05$, ** $p < 0.01$, *** $p < 0.001$.

3.4. SAB Restores PI3K/AKT/mTOR Phosphorylation in the Jejunum of LPS-Challenged Piglets

To examine the association between SAB-mediated epithelial protection and PI3K/AKT/mTOR signaling, we assessed the phosphorylation of PI3K, AKT, and mTOR in the jejunum. LPS challenge suppressed the phosphorylation of PI3K, AKT, and mTOR ($p < 0.05$; Figure 4). SAB supplementation effectively restored their phosphorylation levels ($p < 0.05$), showing that SAB-mediated epithelial protection was accompanied by restored PI3K/AKT/mTOR phosphorylation.

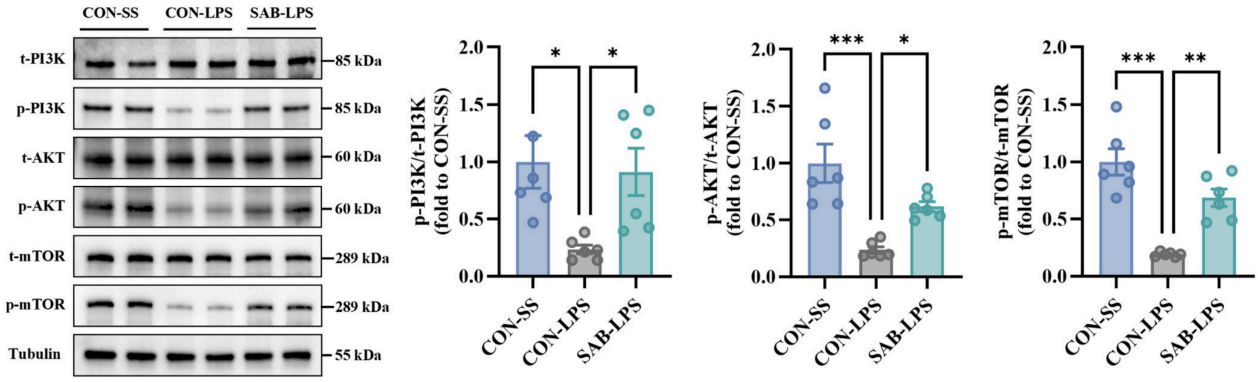


Figure 4. Effects of SAB on PI3K/AKT/mTOR phosphorylation in the jejunum of LPS-challenged piglets. Data are presented as mean ± SEM (n = 6). * $p < 0.05$, ** $p < 0.01$, *** $p < 0.001$.

3.5. LY294002 Treatment Attenuates SAB-Mediated Epithelial Protection in LPS-Stimulated IPEC-J2 Cells

To examine the pharmacological involvement of PI3K/AKT/mTOR signaling in SAB-mediated epithelial protection, LY294002 was used in IPEC-J2 cells. LPS stimulation significantly reduced PI3K, AKT and mTOR phosphorylation relative to untreated cells ($p < 0.05$; Figure 5A). SAB treatment alone did not significantly alter the phosphorylation of these proteins compared with the control group ($p > 0.05$), whereas it significantly restored their phosphorylation levels in LPS-stimulated IPEC-J2 cells ($p < 0.05$). Pretreatment with LY294002 substantially weakened these SAB-induced phosphorylation events ($p < 0.05$).

Further functional analyses showed that LPS stimulation disrupted epithelial barrier integrity, as evidenced by reduced TEER and increased FD4 permeability ($p < 0.05$; Figure 5B,C). LPS also induced marked increases in the mRNA expression of *TNF-α*, *IL-1β*, and *IL-6* ($p < 0.05$; Figure 5D). Moreover, LPS reduced EdU-positive cells, elevated the apoptosis rate, and downregulated the protein expression of occludin and ZO-1 ($p < 0.05$; Figure 5E–G). SAB treatment alone did not significantly affect any of these parameters compared with the control group ($p > 0.05$). However, under LPS-stimulated conditions, SAB treatment significantly reversed these LPS-induced alterations, as reflected by increased TEER, decreased FD4 permeability, suppressed pro-inflammatory cytokine expression, enhanced EdU incorporation, reduced apoptosis, and restored tight junction protein expression ($p < 0.05$). Notably, LY294002 largely weakened the influence of SAB on these parameters ($p < 0.05$), providing pharmacological evidence for the involvement of PI3K/AKT/mTOR signaling in SAB-associated restoration of epithelial barrier integrity.

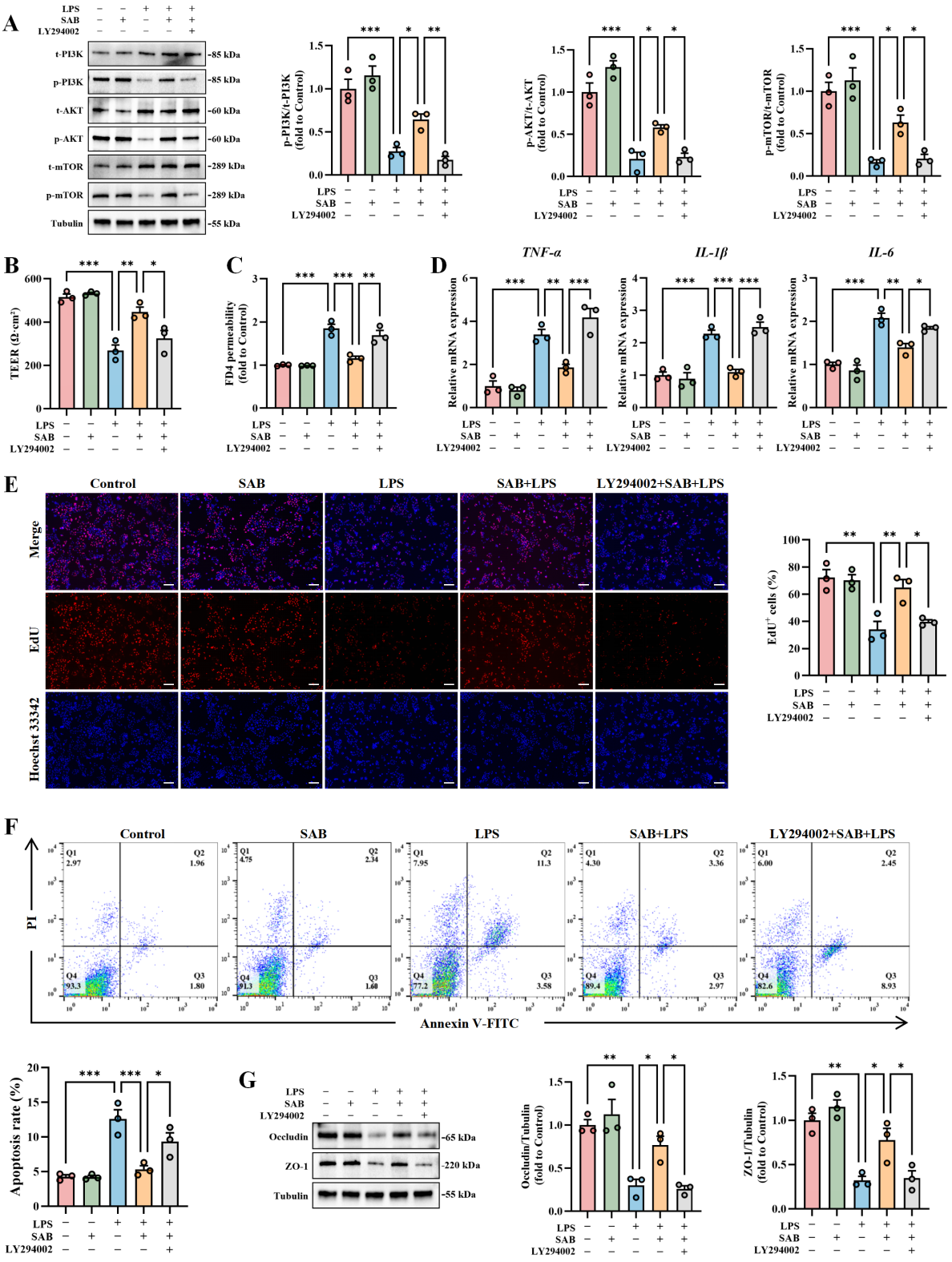


Figure 5. LY294002 treatment weakens SAB-mediated epithelial protection in LPS-stimulated IPEC-J2 cells. (**A**) Representative Western blot bands and quantification of p-PI3K/PI3K, p-AKT/AKT, and p-mTOR/mTOR ratios; (**B**) TEER; (**C**) Paracellular permeability assessed by FD4 flux; (**D**) The mRNA expression of pro-inflammatory cytokines; (**E**) Quantification of EdU-positive cells (scale bar = 200 μm); (**F**) Apoptosis rate; (**G**) Representative Western blot bands and quantification of tight junction proteins. Data are presented as mean ± SEM from three independent biological experiments (n = 3). * $p < 0.05$, ** $p < 0.01$, *** $p < 0.001$.

3.6. Docking and MD Simulations Characterize a Predicted SAB-PI3Kα/p110α Interaction

To explore the interaction between SAB and PI3K, molecular docking simulation was carried out. As illustrated in Figure 6A, SAB was predicted to interact with PI3Kα/p110α, with an AutoDock Vina score of −8.015 kcal/mol. The predicted binding mode was stabilized by six hydrogen bonds, two salt bridges, and hydrophobic interactions. Among the interacting residues, Lys271, located within the RAS-binding domain of p110α, participated in multiple contacts with SAB, suggesting a possible contribution to stabilization of the predicted binding pose.

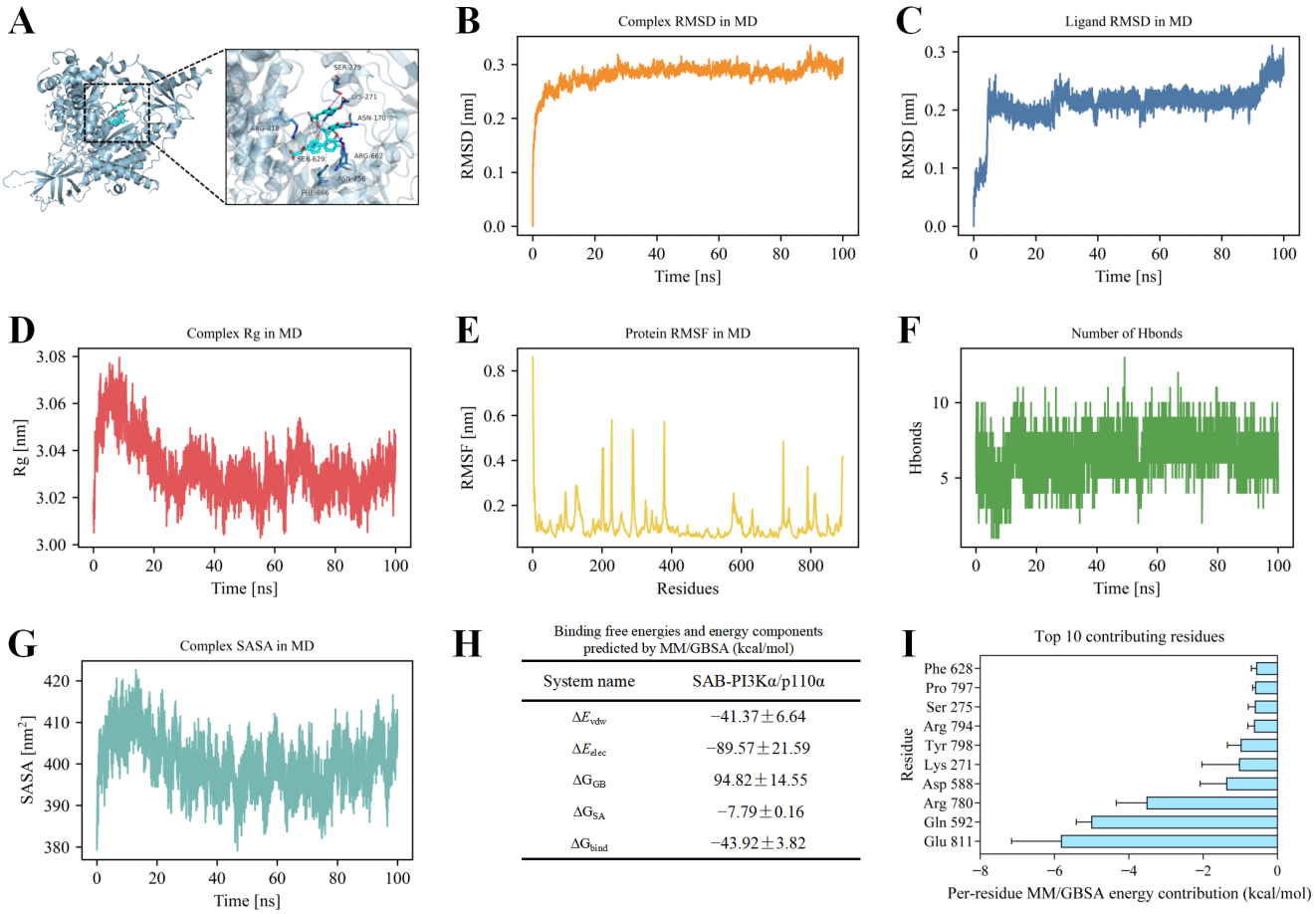


Figure 6. Molecular docking and MD simulation of the predicted SAB-PI3Kα/p110α complex. (**A**) Predicted binding mode between SAB and PI3Kα/p110α, where SAB is shown as cyan sticks and the protein as a blue cartoon. Blue, yellow, and gray dashed lines represent hydrogen bonds, salt bridges, and hydrophobic interactions, respectively; (**B**) RMSD of the SAB-PI3Kα/p110α complex during 100 ns MD simulation; (**C**) RMSD of the SAB ligand; (**D**) Rg of the complex; (**E**) RMSF of protein backbone residues; (**F**) Number of hydrogen bonds formed between SAB and PI3Kα/p110α during the simulation; (**G**) SASA of the complex; (**H**) Binding free energy calculated by MM/GBSA; (**I**) Per-residue binding free energy decomposition.

The stability of the predicted complex was subsequently examined by a 100-ns MD simulation. RMSD of the complex rapidly reached a plateau with only minor fluctuations (Figure 6B), suggesting conformational stability of the predicted complex within the single 100-ns trajectory examined. The ligand RMSD also stabilized after an initial adjustment phase, indicating that SAB was retained within the predicted binding region without major displacement (Figure 6C). In addition, the radius of gyration remained relatively constant after the initial equilibration stage, indicating maintenance of a compact conformation (Figure 6D). RMSF analysis showed limited flexibility across most residues, with higher

fluctuations mainly located in terminal and loop regions (Figure 6E). The hydrogen bond analysis further showed that SAB maintained a dynamic polar interaction network with PI3K throughout the simulation (Figure 6F). SASA values fluctuated within a stable range after initial adjustment, suggesting local surface adaptation without global structural disruption (Figure 6G).

MM/GBSA analysis yielded a model-dependent binding-energy estimate of −43.92 ± 3.82 kcal/mol for the predicted SAB-PI3Kα/p110α complex, suggesting favorable energetics within the computational model (Figure 6H). Energy decomposition suggested that van der Waals and electrostatic interactions were the major contributors to binding, whereas desolvation effects partially counteracted complex formation. Per-residue energy decomposition further showed that several charged, polar, and hydrophobic residues contributed to ligand stabilization, suggesting that the predicted interaction was supported by a coordinated network of polar recognition, electrostatic complementarity, and local hydrophobic contacts (Figure 6I). Overall, these in silico analyses suggest that SAB may form a dynamically stable complex with PI3K through coordinated polar, electrostatic, and hydrophobic interactions.

3.7. SAB Alters the Jejunal Microbiota and Metabolite Profile in LPS-Challenged Piglets

Jejunal microbial communities were characterized by 16S rRNA gene sequencing. Of the detected OTUs, 133 were shared across all three groups, whereas 34, 101, and 78 were unique to the CON-SS, CON-LPS, and SAB-LPS groups, respectively (Figure 7A). Alpha-diversity analysis showed that LPS exposure increased Sobs, Chao, Ace, and Shannon indices, while decreasing the Simpson index ($p < 0.05$; Figure 7B–F). SAB supplementation did not significantly reverse these LPS-induced changes in alpha diversity ($p > 0.05$). PCoA analysis revealed distinct clustering of jejunal microbial communities among the three groups (Figure 7G). Adonis analysis further confirmed significant differences in jejunal microbiota structure between the CON-LPS and CON-SS groups and between the SAB-LPS and CON-LPS groups. These findings suggest that SAB reshaped the jejunal microbial community structure.

Taxonomic analysis suggested that Firmicutes, Proteobacteria, and Actinobacteriota were the predominant phyla in jejunal digesta (Figure 7H). LPS exposure decreased the relative abundance of Firmicutes and increased that of Proteobacteria, whereas SAB supplementation reversed these LPS-induced changes by increasing Firmicutes abundance and decreasing Proteobacteria abundance ($p < 0.05$; Figure 7I). Among the top 25 genera by relative abundance, LPS challenge decreased the relative abundance of *Streptococcus*, while increasing the relative abundances of *Escherichia-Shigella*, *Romboutsia*, *Terrisporobacter*, and *Dietzia* ($p < 0.05$, Figure 7J,K). However, SAB supplementation increased the relative abundance of *Streptococcus* and *Clostridium_sensu_stricto_6* and reduced that of *Escherichia-Shigella, Enterobacter,* and *Actinobacillus* ($p < 0.05$). LEfSe analysis further distinguished treatment-specific microbial signatures (Figure 7L). The CON-SS group was enriched in *Streptococcus*, *Bifidobacterium*, and Firmicutes, whereas *Escherichia-Shigella*, *Romboutsia*, *Terrisporobacter*, and the phylum Proteobacteria were characteristic of the CON-LPS group. The SAB-LPS group exhibited a distinct microbial signature, with enrichment of *Turicibacter*, *Dietzia*, and the phylum Actinobacteriota. These data suggest that SAB altered the jejunal microbiota composition in LPS-challenged piglets.

To further determine whether these microbial alterations were accompanied by changes in the jejunal metabolite profile, SCFA and lactate concentrations were measured. LPS challenge decreased total SCFAs, acetate, propionate, and lactate concentrations compared with the CON-SS group ($p < 0.05$; Figure 7M). In contrast, SAB significantly increased total SCFAs, acetate, and lactate levels compared with the CON-LPS group ($p < 0.05$). These data indicate that SAB partially counteracts LPS-induced disruption of the jejunal organic acid profile.

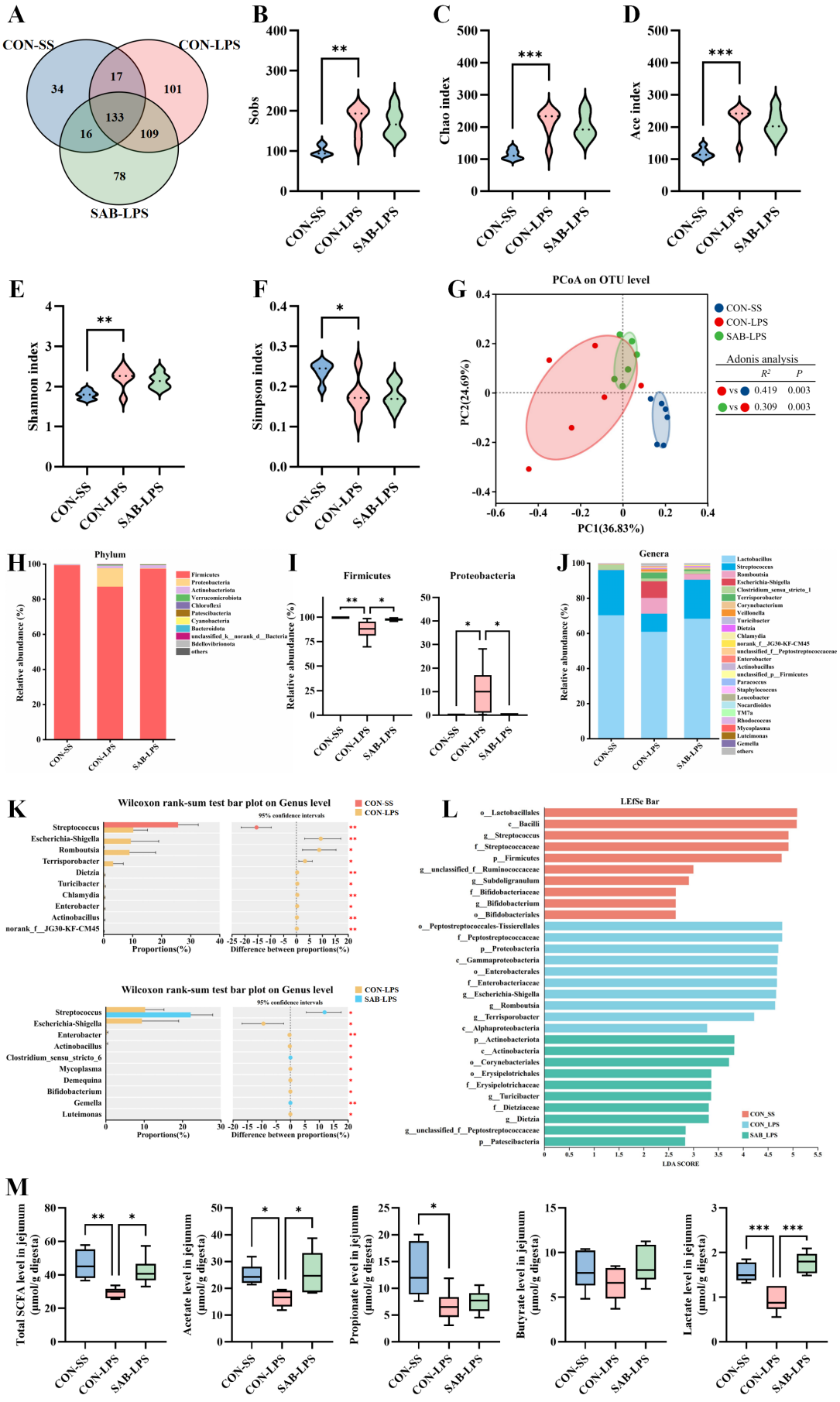


Figure 7. SAB alters the jejunal microbiota and metabolite profile in LPS-challenged piglets. (**A**) Venn diagram of bacterial OTUs; (**B**–**F**) Sobs, Chao, Ace, Shannon, and Simpson indices;

(**G**) PCoA plot based on Bray–Curtis dissimilarity with Adonis analysis; (**H**) Relative abundance of the top 10 bacterial phyla; (**I**) Differentially abundant phyla; (**J**) Relative abundance of the top 25 bacterial genera; (**K**) Differentially abundant genera identified by Wilcoxon rank-sum test; (**L**) LEfSe analysis showing differentially abundant bacterial taxa (LDA score > 2, $p < 0.05$); (**M**) Concentrations of total SCFAs, acetate, propionate, butyrate, and lactate in jejunal digesta. Violin plots (**B**–**F**) show the data distribution, with the horizontal line indicating the median. Box-and-whisker plots (**I**,**M**) show the median, interquartile range, and minimum-to-maximum values ($n = 6$). Significance annotations are based on FDR-adjusted p values. * $p < 0.05$, ** $p < 0.01$, *** $p < 0.001$.

3.8. Associations Among Jejunal Microbiota, Metabolites, and Intestinal Barrier Parameters

Spearman correlation analysis was used to examine relationships among bacterial genera, jejunal metabolites, and host barrier-related variables. At the microbiota–metabolite level, *Streptococcus* abundance was positively associated with acetate, lactate, and total SCFAs. In contrast, *Escherichia-Shigella*, *Enterobacter*, and *Actinobacillus* showed inverse associations with these metabolites ($p < 0.05$; Figure 8A). At the metabolite–intestinal barrier level, total SCFAs were positively correlated with epithelial proliferation and negatively correlated with plasma D-lactate, epithelial apoptosis, and jejunal TNF-α and IL-1β levels. Lactate was positively correlated with epithelial proliferation and negatively correlated with plasma DAO, D-lactate, and TNF-α levels. Acetate was negatively correlated with plasma D-lactate, epithelial apoptosis, and jejunal TNF-α levels ($p < 0.05$; Figure 8B). At the microbiota–host level, *Streptococcus* abundance was positively correlated with epithelial proliferation and negatively correlated with plasma D-lactate, epithelial apoptosis, and jejunal TNF-α levels. Conversely, the abundances of *Escherichia-Shigella* and *Enterobacter* were positively correlated with plasma DAO activity, plasma D-lactate, and jejunal TNF-α and IL-1β levels, but negatively correlated with epithelial proliferation ($p < 0.05$; Figure 8C). Collectively, these findings support an association between SAB-induced microbiota–metabolite remodeling and improved intestinal barrier homeostasis.

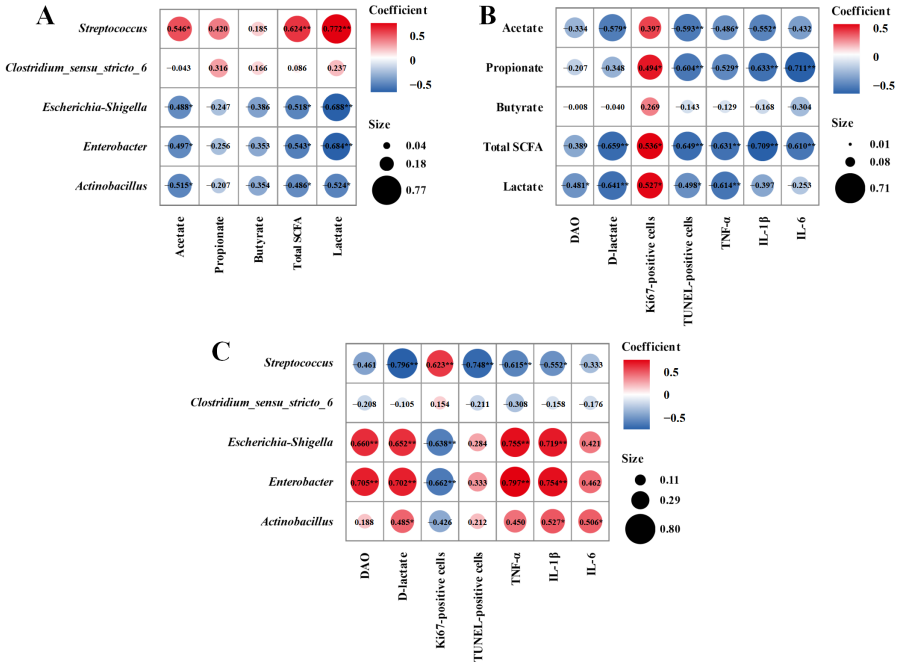


Figure 8. Spearman correlation heatmaps showing associations among key bacterial genera, microbial metabolites, and host intestinal barrier parameters. (**A**) Correlations between key genera and SCFAs/lactate. (**B**) Correlations between SCFAs/lactate and host intestinal homeostasis parameters. (**C**) Correlations between key genera and host intestinal homeostasis parameters. * $p < 0.05$, ** $p < 0.01$.

4. Discussion

Intestinal epithelial barrier damage is a common feature of various enteric disorders, and effective interventions remain limited. In the current study, SAB, a water-soluble phenolic acid identified in *Salvia miltiorrhiza*, attenuated LPS-induced jejunal barrier dysfunction, morphological disruption, and inflammation in piglets. This protection was associated with restoration of PI3K/AKT/mTOR-associated epithelial proliferation–apoptosis balance and remodeling of the jejunal microbiota–metabolite profile. Our findings therefore provide mechanistic evidence supporting the functional potential of SAB in maintaining intestinal barrier homeostasis under inflammatory stress.

As the first defense against luminal pathogens and harmful substances, the intestinal barrier plays a vital role in maintaining immune homeostasis and overall health [31,32]. Here, SAB reduced plasma DAO and D-lactate levels, restored jejunal villus morphology, and lowered histopathological injury scores of LPS-challenged piglets. These in vivo observations were further supported by in vitro evidence showing that SAB alleviated LPS-induced TEER reduction and FD4 hyperpermeability in IPEC-J2 cells, indicating that SAB preserves epithelial barrier integrity. The intestinal barrier relies on tight junctions and the mucus layer to restrict luminal threats. Tight junction proteins restrict paracellular permeation by sealing the intercellular space, while the mucus layer, rich in goblet cell-derived mucin 2, prevents direct bacterial–epithelial contact [33]. Previous work showed that SAB restores tight junction protein expression in the colon of 2,4,6-trinitrobenzenesulfonic acid-challenged rats via the miR-1/MLCK pathway [34]. Consistent with these findings, SAB restored occludin and ZO-1 expression in the jejunum of LPS-challenged piglets and in LPS-stimulated IPEC-J2 cells. Meanwhile, SAB reinforced the jejunal mucus barrier by preserving goblet cell abundance and mucin 2 levels in LPS-challenged piglets. These barrier-protective effects may reduce epithelial exposure to luminal antigens and microbial products and thereby limit amplification of mucosal inflammation.

Continuous epithelial turnover is essential for preserving intestinal structure, and an imbalance between proliferation and apoptosis can impair mucosal renewal and contribute to villus atrophy [35]. In this study, SAB treatment increased Ki67-positive cells, upregulated proliferation-associated genes *PCNA* and the anti-apoptotic gene *BCL2*, while decreasing TUNEL-positive cells and suppressing the pro-apoptotic gene *BAX*, indicating that SAB shifts the balance toward enhanced epithelial renewal. Given the single 6-h endpoint, these findings primarily reflect early changes in epithelial proliferation and apoptosis. It is reported that PI3K/AKT signaling integrates growth and metabolic cues involved in epithelial proliferation and repair [36]. The ability of SAB to activate this pathway has been documented in several other experimental settings. For instance, SAB reduces ototoxic drug-induced hair cell apoptosis through PI3K/AKT signaling [37]. SAB also improves blood perfusion and promotes M2 macrophage polarization via the SIRT1/PI3K/AKT pathway in a mouse model of limb ischemia [38]. Here, SAB restored the phosphorylation of PI3K, AKT, and mTOR in both the jejunum of LPS-challenged piglets and LPS-treated IPEC-J2 cells. Moreover, LY294002 treatment attenuated the SAB-induced increases in PI3K, AKT and mTOR phosphorylation and weakened the restoration of epithelial proliferation–apoptosis balance and barrier integrity, as well as the suppression of inflammatory responses, in LPS-treated IPEC-J2 cells. These findings provide pharmacological evidence supporting the involvement of PI3K/AKT/mTOR signaling in SAB-mediated epithelial protection. Nevertheless, since the present evidence is based on pathway phosphorylation and a single pharmacological inhibitor, additional genetic or independent pharmacological approaches are required to establish pathway-specific causality.

Interestingly, molecular docking and MD simulations of this study provided a structural hypothesis for the interaction between SAB and PI3Kα/p110α. SAB was predicted

to interact with PI3K and form a relatively stable complex supported by hydrogen bonds, salt bridges, hydrophobic contacts, and favorable binding energetics. Among the predicted interacting residues, Lys271 may contribute to ligand stabilization. These in silico findings are consistent with the observed restoration of PI3K/AKT/mTOR signaling by SAB and the attenuation of SAB-mediated protection by LY294002. Nevertheless, direct biochemical validation will be required to determine whether SAB physically engages PI3K and modulates its kinase activity.

Growing evidence supports that the gut microbiota is closely associated with intestinal barrier integrity, immune responses, and host metabolism [39,40]. In this study, LPS exposure elevated several alpha-diversity indices of the jejunal microbiota, and these changes were not significantly reversed by SAB. This pattern may reflect a transient expansion of specific jejunal taxa under inflammatory challenge rather than a uniform loss of microbial richness [41]. In contrast, PCoA and Adonis analysis showed clear separation among groups, particularly between CON-LPS and SAB-LPS, implying that SAB reshapes the ecological structure of the jejunal microbiota. At the phylum level, LPS decreased the relative abundance of Firmicutes and increased that of Proteobacteria, consistent with changes previously reported in the jejunum of LPS-challenged piglets [42]. SAB shifted the relative abundances of both phyla toward the control profile. Firmicutes and Proteobacteria were the predominant phyla in the jejunal microbiota of piglets [42]. Given the broad taxonomic and functional heterogeneity within these phyla, these shifts may be attributed to community-level compositional signatures associated with LPS challenge and SAB treatment. At the genus level, LPS challenge was associated with broader compositional changes involving *Streptococcus*, *Escherichia-Shigella*, *Romboutsia*, *Terrisporobacter*, and *Dietzia*. Similarly, SAB treatment was associated with changes in several genera, including *Streptococcus*, *Escherichia-Shigella*, *Clostridium_sensu_stricto_6*, *Enterobacter*, and *Actinobacillus*. Thus, SAB did not simply normalize individual LPS-responsive taxa but mediated a broader reorganization of the jejunal microbial community. Among these changes, SAB increased the relative abundance of *Streptococcus* and decreased that of the *Escherichia-Shigella* group. *Streptococcus* is frequently detected as an abundant genus in the piglet jejunum [43], while increased *Escherichia-Shigella* abundance has also been observed in LPS-challenged piglets and other inflammatory conditions [42,44]. Interestingly, correlation analysis in this study showed that *Streptococcus* abundance was positively associated with jejunal acetate and lactate concentrations and epithelial proliferation, and negatively associated with indicators of barrier injury, apoptosis, and inflammation. The *Escherichia-Shigella* group exhibited the opposite correlation pattern. These coordinated changes indicate an association among jejunal microbial composition, metabolite concentrations, and epithelial status following SAB treatment. However, the genus-level resolution of 16S rRNA sequencing does not establish the metabolic contribution or causal role of individual taxa. Future studies combining shotgun metagenomic sequencing with microbiota- and metabolite-targeted interventions are needed to clarify the contribution of these alterations to SAB-mediated barrier protection.

Notably, several microbial groups whose relative abundances were altered following SAB treatment in the piglet jejunum are also commonly detected in the human small-intestinal microbiota, including Firmicutes, Proteobacteria, and Streptococcal and Enterobacterial taxa [45,46]. Recent studies further indicate that the human small-intestinal microbiota is spatially dynamic and responsive to nutritional interventions [47]. However, because no direct cross-species comparison was performed, the present study cannot determine whether microbial diversity and taxon relative abundances are quantitatively comparable between pigs and humans. This taxonomic overlap therefore provides only qualitative ecological context, and further studies are required to determine whether SAB induces similar microbial and metabolic changes in humans.

5. Conclusions

SAB attenuated LPS-induced intestinal inflammation and barrier injury and restored epithelial proliferation–apoptosis balance, with pharmacological inhibition supporting PI3K/AKT/mTOR involvement in these effects. SAB also changed the jejunal microbiota and metabolite profile, as reflected by higher relative abundances of Firmicutes and *Streptococcus*, lower relative abundances of Proteobacteria and *Escherichia-Shigella*, and increased acetate and lactate concentrations. Collectively, these findings support the potential of SAB as a plant-derived dietary bioactive compound for protecting intestinal barrier function under inflammatory stress.

Supplementary Materials: The following supporting information can be downloaded at: https://www.mdpi.com/article/10.3390/antiox15111425/s1, Supplementary methods: Detailed description of sample collection, assessment of epithelial barrier function, molecular docking and MD simulations, determination of jejunal SCFAs and lactate; Table S1: Composition and nutrient levels of the basal diet (air-dry basis); Table S2: Antibody information; Table S3: Primer sequences for quantitative real-time PCR; Figure S1: Cytotoxicity assessment and selection of the working concentration of SAB in IPEC-J2 cells. Figure S2: Effects of LY294002 on cell viability and AKT/mTOR phosphorylation in IPEC-J2 cells.

Author Contributions: Conceptualization: Y.C. Formal analysis: Y.J. and H.X. Investigation: Y.J., H.X. and J.Z. Data curation: Y.J. and H.X. Writing—original draft: Y.J. and H.X. Methodology: H.Z. and J.Z. Validation: H.Z. and H.W. Funding acquisition: H.Z. and Y.C. Project administration: Y.C. Supervision: Y.Y., Y.C., H.W., C.L. and Q.Y. Writing—review and editing: Y.C. and H.W. All authors have read and agreed to the published version of the manuscript.

Funding: This work was supported by the Natural Science Foundation of Jiangsu Province (BK20240671), the National Natural Science Foundation of China (32272917), and the Jiangsu Provincial Young Science and Technology Talent Support Program (JSTJ-2024-456).

Institutional Review Board Statement: The animal study protocol was approved by the Institutional Animal Care and Use Committee of Nanjing Forestry University (approval no. 2024020; date of approval: 11 March 2024).

Informed Consent Statement: Not applicable.

Data Availability Statement: The raw 16S rRNA gene sequencing data generated in this study have been deposited in the NCBI Sequence Read Archive under BioProject accession number PRJNA1519105. Other data supporting the findings of this study are available from the corresponding author upon reasonable request.

Conflicts of Interest: The authors declare no conflicts of interest.

References

1. Neurath, M.F.; Artis, D.; Becker, C. The intestinal barrier: A pivotal role in health, inflammation, and cancer. *Lancet Gastroenterol. Hepatol.* **2025**, *10*, 573–592. [CrossRef]
2. Horowitz, A.; Chanez-Paredes, S.D.; Haest, X.; Turner, J.R. Paracellular permeability and tight junction regulation in gut health and disease. *Nat. Rev. Gastroenterol. Hepatol.* **2023**, *20*, 417–432. [CrossRef]
3. Yeshi, K.; Jamtsho, T.; Wangchuk, P. Current treatments, emerging therapeutics, and natural remedies for inflammatory bowel disease. *Molecules* **2024**, *29*, 3954. [CrossRef]
4. Muro, P.; Zhang, L.; Li, S.; Zhao, Z.; Jin, T.; Mao, F.; Mao, Z. The emerging role of oxidative stress in inflammatory bowel disease. *Front. Endocrinol.* **2024**, *15*, 1390351. [CrossRef]
5. Arumugam, P.; Saha, K.; Nighot, P. Intestinal epithelial tight junction barrier regulation by novel pathways. *Inflamm. Bowel Dis.* **2025**, *31*, 259–271. [CrossRef]
6. Parker, A.; Vaux, L.; Patterson, A.M.; Modasia, A.; Muraro, D.; Fletcher, A.G.; Byrne, H.M.; Maini, P.K.; Watson, A.J.M.; Pin, C. Elevated apoptosis impairs epithelial cell turnover and shortens villi in TNF-driven intestinal inflammation. *Cell Death Dis.* **2019**, *10*, 108. [CrossRef]

7. He, Y.; Sun, M.; Zhang, G.; Yang, J.; Chen, K.; Xu, W.; Li, B. Targeting PI3K/Akt signal transduction for cancer therapy. *Signal Transduct. Target. Ther.* **2021**, *6*, 425. [CrossRef]
8. Glaviano, A.; Foo, A.S.C.; Lam, H.Y.; Yap, K.C.H.; Jacot, W.; Jones, R.H.; Eng, H.; Nair, M.G.; Makvandi, P.; Geoerger, B.; et al. PI3K/AKT/mTOR signaling transduction pathway and targeted therapies in cancer. *Mol. Cancer* **2023**, *22*, 138. [CrossRef]
9. Kaur, H.; Moreau, R. Role of mTORC1 in intestinal epithelial repair and tumorigenesis. *Cell. Mol. Life Sci.* **2019**, *76*, 2525–2546. [CrossRef]
10. Zhang, X.; Zhang, F.; Li, Y.; Fan, N.; Zhao, K.; Zhang, A.; Kang, J.; Lin, Y.; Xue, X.; Jiang, X. Blockade of PI3K/AKT signaling pathway by astragaloside IV attenuates ulcerative colitis via improving the intestinal epithelial barrier. *J. Transl. Med.* **2024**, *22*, 406. [CrossRef]
11. de Vos, W.M.; Tilg, H.; Van Hul, M.; Cani, P.D. Gut microbiome and health: Mechanistic insights. *Gut* **2022**, *71*, 1020–1032. [CrossRef]
12. Mann, E.R.; Lam, Y.K.; Uhlig, H.H. Short-chain fatty acids: Linking diet, the microbiome and immunity. *Nat. Rev. Immunol.* **2024**, *24*, 577–595. [CrossRef]
13. Lavelle, A.; Sokol, H. Gut microbiota-derived metabolites as key actors in inflammatory bowel disease. *Nat. Rev. Gastroenterol. Hepatol.* **2020**, *17*, 223–237. [CrossRef]
14. Parada Venegas, D.; De la Fuente, M.K.; Landskron, G.; González, M.J.; Quera, R.; Dijkstra, G.; Harmsen, H.J.M.; Faber, K.N.; Hermoso, M.A. Short chain fatty acids (SCFAs)-mediated gut epithelial and immune regulation and its relevance for inflammatory bowel diseases. *Front. Immunol.* **2019**, *10*, 277, Correction in *Front. Immunol.* **2019**, *10*, 1486. [CrossRef]
15. He, G.; Chen, G.; Liu, W.; Ye, D.; Liu, X.; Liang, X.; Song, J. Salvianolic acid B: A review of pharmacological effects, safety, combination therapy, new dosage forms, and novel drug delivery routes. *Pharmaceutics* **2023**, *15*, 2235. [CrossRef]
16. Liang, Q.; Liu, X.; Peng, X.; Luo, T.; Su, Y.; Xu, X.; Xie, H.; Gao, H.; Chen, Z.; Xie, C. Salvianolic acid B in fibrosis treatment: A comprehensive review. *Front. Pharmacol.* **2024**, *15*, 1442181. [CrossRef]
17. Fei, R.; Wang, S.; Shang, T. Salvianolic acid B regulates intestinal bacterial/endotoxin translocation after intestinal ischemia/reperfusion injury in rats through TLR4/MyD88/MAPK pathway. *J. Biochem. Mol. Toxicol.* **2025**, *39*, e70551. [CrossRef]
18. Wang, H.; Zhang, H.; Lai, C.; Chen, Y. Salvianolic acid B ameliorates lipopolysaccharide-induced inflammatory liver injury via deacetylation of NF-κB RelA. *Food Biosci.* **2025**, *68*, 106794, Correction in *Food Biosci.* **2026**, *77*, 108342. [CrossRef]
19. Zhao, Y.; Shao, C.; Zhou, H.; Yu, L.; Bao, Y.; Mao, Q.; Yang, J.; Wan, H. Salvianolic acid B inhibits atherosclerosis and TNF-α-induced inflammation by regulating NF-κB/NLRP3 signaling pathway. *Phytomedicine* **2023**, *119*, 155002. [CrossRef]
20. Wu, X.; Wang, L.; Tang, L.; Wang, L.; Cao, S.; Wu, Q.; Zhang, Z.; Li, L. Salvianolic acid B alters the gut microbiota and mitigates colitis severity and associated inflammation. *J. Funct. Foods* **2018**, *46*, 312–319. [CrossRef]
21. Raetz, C.R.H.; Whitfield, C. Lipopolysaccharide endotoxins. *Annu. Rev. Biochem.* **2002**, *71*, 635–700. [CrossRef]
22. Lunney, J.K.; Van Goor, A.; Walker, K.E.; Hailstock, T.; Franklin, J.; Dai, C. Importance of the pig as a human biomedical model. *Sci. Transl. Med.* **2021**, *13*, eabd5758. [CrossRef]
23. Sun, X.; Cui, Y.; Su, Y.; Gao, Z.; Diao, X.; Li, J.; Zhu, X.; Li, D.; Li, Z.; Wang, C.; et al. Dietary fiber ameliorates lipopolysaccharide-induced intestinal barrier function damage in piglets by modulation of intestinal microbiome. *mSystems* **2021**, *6*, e01374-20. [CrossRef]
24. Zheng, X.; Wang, Y.; Zhou, X.; Deng, T.; Zhao, Y.; Fu, Z.; Wei, Y.; Ma, W.; Zhang, S.; Guan, W.; et al. Plant essential oils combined with organic acids restored lipopolysaccharide-induced leaky intestine via gut microbial modulation in weaned piglets. *Anim. Nutr.* **2024**, *18*, 419–432. [CrossRef]
25. Mao, J.; Qi, S.; Cui, Y.; Dou, X.; Luo, X.M.; Liu, J.; Zhu, T.; Ma, Y.; Wang, H. Lactobacillus rhamnosus GG attenuates lipopolysaccharide-induced inflammation and barrier dysfunction by regulating MAPK/NF-κB signaling and modulating metabolome in the piglet intestine. *J. Nutr.* **2020**, *150*, 1313–1323. [CrossRef]
26. Tian, S.; Wang, J.; Gao, R.; Wang, J.; Zhu, W. Early-life galacto-oligosaccharides supplementation alleviates the small intestinal oxidative stress and dysfunction of lipopolysaccharide-challenged suckling piglets. *J. Anim. Sci. Biotechnol.* **2022**, *13*, 70. [CrossRef]
27. Li, Y.; Zhang, H.; Feng, T.; Cao, J.; Hou, X.; Chen, Y.; Yan, J. Effects of resveratrol and its derivative pterostilbene on hepatic injury and immunological stress of weaned piglets challenged with lipopolysaccharide. *J. Anim. Sci.* **2022**, *100*, skac339. [CrossRef]
28. Wang, H.; Dou, X.; Wang, R.; Jiang, Y.; Zhang, J.; Qiao, X.; Liu, Y.; Zhang, H.; Lai, C.; Chen, Y.; et al. Salvianolic acid B alleviates LPS-induced spleen injury by remodeling redox status and suppressing NLRP3 inflammasome. *Antioxidants* **2025**, *14*, 883. [CrossRef]
29. Gu, X.; Guo, W.; Zhao, Y.; Liu, G.; Wu, J.; Chang, C. Deoxynivalenol-induced cytotoxicity and apoptosis in IPEC-J2 cells through the activation of autophagy by inhibiting PI3K-AKT-mTOR signaling pathway. *ACS Omega* **2019**, *4*, 18478–18486. [CrossRef]
30. Zhou, L.; Tang, Z.; Lin, Y.; Zhou, T.; Shen, M.; Lin, Y.; Chen, C.; Chen, C. A novel curcumin analog sAc15 alleviates LPS-induced acute lung injury by activating the PI3K/AKT/Nrf2 pathway in pulmonary epithelial cells. *Redox Rep.* **2026**, *31*, 2721883. [CrossRef]
31. Peterson, L.W.; Artis, D. Intestinal epithelial cells: Regulators of barrier function and immune homeostasis. *Nat. Rev. Immunol.* **2014**, *14*, 141–153. [CrossRef]

32. Chen, Q.; Yang, L.; Xiang, F.; Szeto, I.M.Y.; Yan, Y.; Liu, B.; Cheng, J.; Liu, L.; Li, B.; Duan, S. 2′-Fucosyllactose modulates the function of intestinal microbiota to reduce intestinal permeability in mice colonized by feces from healthy infants. *Food Sci. Hum. Wellness* **2025**, *14*, 9250021. [CrossRef]
33. Gustafsson, J.K.; Hansson, G.C. Immune regulation of goblet cell and mucus functions in health and disease. *Annu. Rev. Immunol.* **2025**, *43*, 169–189. [CrossRef]
34. Xiong, Y.; Wang, J.; Chu, H.; Chen, D.; Guo, H. Salvianolic acid B restored impaired barrier function via downregulation of MLCK by microRNA-1 in rat colitis model. *Front. Pharmacol.* **2016**, *7*, 134. [CrossRef]
35. Kim, M.; Park, Y.; Kim, Y.S.; Ko, S. Cellular plasticity in gut and liver regeneration. *Gut Liver* **2024**, *18*, 949–960. [CrossRef]
36. Rath, E.; Haller, D. Intestinal epithelial cell metabolism at the interface of microbial dysbiosis and tissue injury. *Mucosal Immunol.* **2022**, *15*, 595–604. [CrossRef]
37. Zheng, Z.; Wang, Y.; Yu, H.; Li, W.; Wu, J.; Cai, C.; He, Y. Salvianolic acid B inhibits ototoxic drug-induced ototoxicity by suppression of the mitochondrial apoptosis pathway. *J. Cell. Mol. Med.* **2020**, *24*, 6883–6897. [CrossRef]
38. Niu, W.; Wu, F.; Cao, W.; Chen, Y.; Zhang, Y.; Chen, Y.; Ding, R.; Liang, C. Salvianolic acid B alleviates limb ischemia in mice via promoting SIRT1/PI3K/AKT pathway-mediated M2 macrophage polarization. *Evid.-Based Complement. Altern. Med.* **2022**, *2022*, 1112394. [CrossRef]
39. Fan, Y.; Pedersen, O. Gut microbiota in human metabolic health and disease. *Nat. Rev. Microbiol.* **2021**, *19*, 55–71. [CrossRef]
40. Yu, W.; Zhao, Y.; Zhang, Y.; Li, Y.; Yang, Y.; Wang, J.; Wang, H.; Shi, H.; Xiao, C.; Zhao, M.; et al. Gut microbial metabolites-mediated modulation of colitis in mice by three geographically varied dietary patterns. *Food Sci. Hum. Wellness* **2025**, *14*, 9250420. [CrossRef]
41. Zeng, M.Y.; Inohara, N.; Núñez, G. Mechanisms of inflammation-driven bacterial dysbiosis in the gut. *Mucosal Immunol.* **2017**, *10*, 18–26. [CrossRef]
42. Li, C.; Wang, Y.; Zhao, X.; Li, J.; Wang, H.; Ren, Y.; Sun, H.; Zhu, X.; Song, Q.; Wang, J. Comparative analysis of intestinal inflammation and microbiota dysbiosis of LPS-challenged piglets between different breeds. *Animals* **2024**, *14*, 665. [CrossRef]
43. Correa, F.; Luise, D.; Bosi, P.; Trevisi, P. Weaning differentially affects the maturation of piglet peripheral blood and jejunal Peyer's patches. *Sci. Rep.* **2022**, *12*, 1604. [CrossRef]
44. Bin, P.; Tang, Z.; Liu, S.; Chen, S.; Xia, Y.; Liu, J.; Wu, H.; Zhu, G. Intestinal microbiota mediates enterotoxigenic Escherichia coli-induced diarrhea in piglets. *BMC Vet. Res.* **2018**, *14*, 385. [CrossRef]
45. Leite, G.G.S.; Weitsman, S.; Parodi, G.; Celly, S.; Sedighi, R.; Sanchez, M.; Morales, W.; Villanueva-Millan, M.J.; Barlow, G.M.; Mathur, R.; et al. Mapping the segmental microbiomes in the human small bowel in comparison with stool: A REIMAGINE study. *Dig. Dis. Sci.* **2020**, *65*, 2595–2604. [CrossRef]
46. Shalon, D.; Culver, R.N.; Grembi, J.A.; Folz, J.; Treit, P.V.; Shi, H.; Rosenberger, F.A.; Dethlefsen, L.; Meng, X.; Yaffe, E.; et al. Profiling the human intestinal environment under physiological conditions. *Nature* **2023**, *617*, 581–591. [CrossRef]
47. An, R.; Wilms, E.; Gerritsen, J.; Kim, H.K.; Seguí Pérez, C.; Besseling-van der Vaart, I.; Jonkers, D.M.A.E.; Rijkers, G.T.; de Vos, W.M.; Masclee, A.A.M.; et al. Spatio-temporal dynamics of the human small intestinal microbiome and its response to a synbiotic. *Gut Microbes* **2024**, *16*, 2350173. [CrossRef]

Disclaimer/Publisher's Note: The statements, opinions and data contained in all publications are solely those of the individual author(s) and contributor(s) and not of MDPI and/or the editor(s). MDPI and/or the editor(s) disclaim responsibility for any injury to people or property resulting from any ideas, methods, instructions or products referred to in the content.